arXiv:2508.12261v2 [cs.CV] 20 Aug 2025

Superpixel-informed Continuous Low-Rank Tensor Representation for Multi-Dimensional Data Recovery

Zhizhou Wang[1], Jianli Wang[1]*, Ruijing Zheng[1], Zhenyu Wu[1],

[1]School of Computing and Artificial Intelligence, Southwest Jiaotong University

jenojeff66@gmail.com, wangjianli_123@163.com, zhengxiaodou666@gmail.com, wuzhenyu_961@126.com,

Abstract

Low-rank tensor representation (LRTR) has emerged as a powerful tool for multi-dimensional data processing. However, classical LRTR-based methods face two critical limitations: (1) they typically assume that the holistic data is low-rank; this assumption is often violated in real-world scenarios with significant spatial variations; and (2) they are constrained to discrete meshgrid data, limiting their flexibility and applicability. To overcome these limitations, we propose a Superpixel-informed Continuous Low-Rank Tensor Representation (SCTR) framework, which enables continuous and flexible modeling of multi-dimensional data beyond traditional grid-based constraints. Our approach introduces two main innovations: First, motivated by the observation that semantically coherent regions exhibit stronger low-rank characteristics than holistic data, we employ superpixels as the basic modeling units. This design both encodes rich semantic information and enhances adaptability to diverse forms of data streams. Second, we propose a novel Asymmetric Low-rank Tensor Factorization (ALTF) where superpixel-specific factor matrices are parameterized by a shared neural network with specialized heads. By strategically separating global pattern learning from local adaptation, this framework efficiently captures both cross-superpixel commonalities and within-superpixel variations. This yields a representation that is both highly expressive and compact, balancing computational efficiency with representational adaptability. Extensive experiments on several benchmark datasets demonstrate that SCTR achieves significant improvements, with PSNR gains of 3-5 dB on multispectral images, and consistently outperforms state-of-the-art methods on videos and color images.

Introduction

Multi-dimensional data processing has become fundamental to modern computer vision and signal processing, with applications spanning from medical imaging to autonomous driving. The proliferation of high-dimensional data from advanced sensors—including hyperspectral images, video sequences, and volumetric scans—has established tensor-based methods as indispensable tools for data analysis. Classical tensor decompositions such as Tucker (Kolda and Bader 2009) and CANDECOMP/PARAFAC (CP) (Kolda and Bader 2009) have demonstrated remarkable success in essential tasks including image inpainting (Jiang et al. 2020), denoising (Gong, Chen, and Chen 2020), and compressed sensing (Liu et al. 2019; Zhang and Zheng 2025; Jiang et al. 2024). Recent advances explore tensor network decompositions including Tensor Train (TT) (Oseledets 2011), Tensor Ring (TR) (Li and So 2021), and tubal-rank via tensor-SVD (Kilmer and Martin 2011; Liu et al. 2024) for more efficient low-rank approximations (Bengua et al. 2017; Wang, Aggarwal, and Aeron 2017; Zheng et al. 2021).

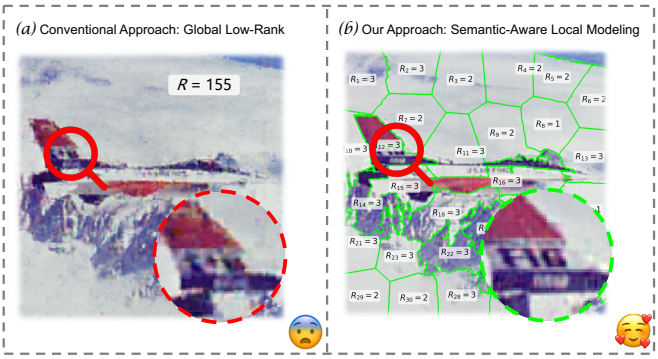


Figure 1: Motivation for SCTR Framework. **(a)** The global method results in a high rank (R=155), contradicting its low-rank assumption. **(b)** In contrast, the low-rank property (R=1-3) of superpixels strongly supports our local hypothesis.

Despite their success, existing tensor methods face two critical challenges that severely limit real-world deployment. First, most approaches assume global low-rank structure across entire tensors, an assumption that breaks down when data contains spatially heterogeneous regions with varying complexities. Natural images typically contain both uniform regions (backgrounds, sky) that are genuinely low-rank alongside complex regions (architectural details, vegetation boundaries) requiring higher-order representations. This creates a fundamental trade-off: use low global rank and lose structural details, or increase global rank and waste computation on simple regions (Liu et al. 2013a; Zhang et al. 2014). As illustrated in Figure 1, conventional methods force the entire image to adopt a uniform high rank to accommodate complex regions,

*Corresponding author

Copyright © 2026, Association for the Advancement of Artificial Intelligence (www.aaai.org). All rights reserved.

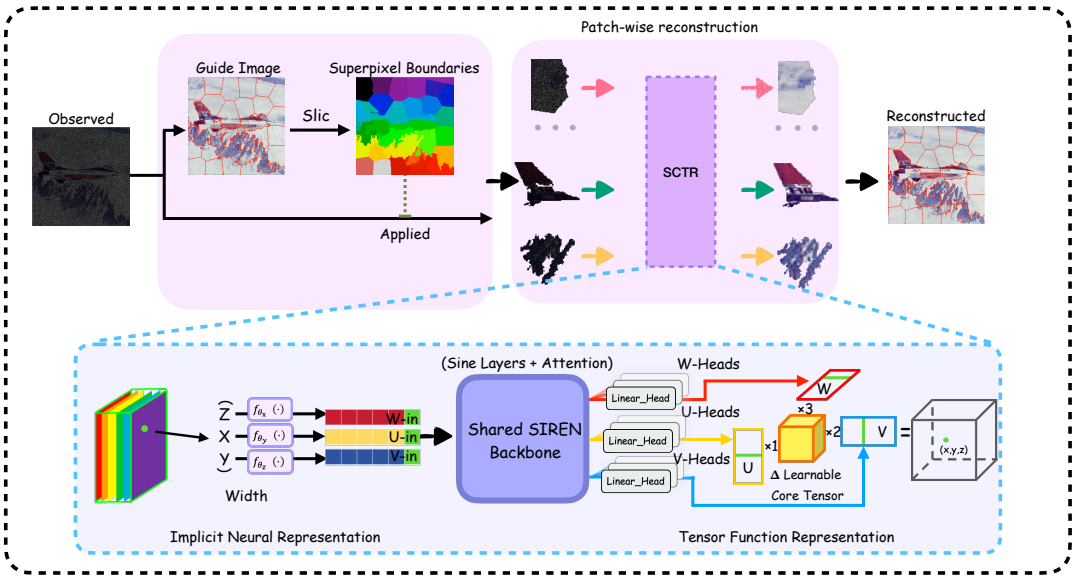


Figure 2: SCTR Framework Overview. **Top**: Superpixel-guided reconstruction pipeline showing semantic segmentation followed by patch-wise tensor completion. **Bottom**: ALTF architecture featuring a shared SIREN backbone that generates coordinate features for specialized heads. These heads predict factor matrices (U, V, W), which combine with learnable core tensors to synthesize output patches via Tucker decomposition.

leading to significant parameter waste in simple areas. Second, traditional tensor methods are inherently designed for discrete, regularly-sampled data, precluding their use in applications requiring continuous representations or irregular sampling patterns. This discrete limitation becomes particularly problematic in modern applications such as neural radiance fields, point cloud processing, and adaptive sensor networks.

Recent efforts have attempted to address these limitations through different approaches. Implicit Neural Representations (INRs) (Sitzmann, Zollhöfer, and Wetzstein 2019; Sitzmann et al. 2020; Chen et al. 2021; Essakine et al. 2025) enable continuous modeling by training neural networks to map coordinates to signal values, allowing representation at arbitrary resolutions. However, conventional INRs struggle with global structure preservation and are prone to overfitting with sparse observations. While S-INR (Li et al. 2024) enhances INR expressiveness through superpixel-based attention mechanisms, it does not address tensor methods' fundamental global low-rank assumptions. These approaches particularly fail to exploit the structural regularities that tensor decomposition naturally captures (Chen, Liu, and Wang 2021; Park et al. 2021).Meanwhile, recent efforts to combine tensor decomposition with neural networks (Wang et al. 2025; Newman et al. 2024; Chen et al. 2022; Zhao et al. 2024; Vemuri, Büchner, and Denzler 2025) primarily focus on optimizing network architectures rather than addressing the fundamental discrete-continuous divide in data representation itself. These hybrid approaches still inherit the global low-rank assumption and discrete grid constraints of classical tensor methods.

To address these limitations, we propose the Superpixel-informed Continuous Low-Rank Tensor Representation (SCTR) framework. The key insight of our work is that instead of imposing a global low-rank assumption, which is often violated in practice, we identify semantically coherent regions and model each separately using continuous representations. As shown in Figure 1(b), our semantic-aware approach naturally discovers that different regions require vastly different ranks, enabling efficient parameter allocation. This "divide-and-conquer" approach naturally accommodates spatial heterogeneity while preserving the computational benefits of low-rank modeling. We implement this insight through the Asymmetric Low-rank Tensor Factorization (ALTF) mechanism, where each superpixel's factor matrices are parameterized through a shared neural network that captures cross-superpixel commonalities and specialized lightweight heads that generate locally-adapted factors.

The main contributions of this paper are:

1. **Local Low-rank Modeling**: We demonstrate that superpixel-based decomposition significantly outperforms global approaches by exploiting natural semantic structure, achieving standout performance with up to 3-5 dB PSNR improvements on multispectral images, while also delivering leading results on video and color image recovery tasks.
2. **Continuous Tensor Representation**: We introduce Asymmetric Low-rank Tensor Factorization (ALTF), a novel method enabling continuous tensor modeling through shared neural networks with specialized local adaptations, thereby bridging the discrete-continuous divide.
3. **Unified Framework**: SCTR provides a unified solution that seamlessly handles diverse data modalities while

Sampling rate		0.05 (5%)		0.10 (10%)		0.15 (15%)		0.20 (20%)		0.25 (25%)	
Data	Method	PSNR	SSIM	PSNR	SSIM	PSNR	SSIM	PSNR	SSIM	PSNR	SSIM
MSIs	LRTFR	36.41	0.7707	42.03	0.9259	44.65	0.9595	45.87	0.9681	46.60	0.9728
Face	CRNL	36.15	0.9669	40.42	0.9859	43.64	0.9922	46.66	0.9954	48.77	0.9967
Flowers	FCTN	26.34	0.7176	36.88	0.9325	41.58	0.9657	43.45	0.9758	44.36	0.9797
Toy	TNN	30.31	0.8438	34.27	0.9197	37.21	0.9527	39.34	0.9693	41.21	0.9790
Painting	t-CTV	33.80	0.9643	37.91	0.9867	40.75	0.9939	43.08	**0.9970**	44.93	**0.9984**
Beers	SCTR	**41.92**	**0.9775**	**45.80**	**0.9904**	**48.38**	**0.9943**	**49.40**	0.9952	**50.23**	0.9958
Videos	LRTFR	25.03	0.6673	26.38	0.7248	26.84	0.7464	27.04	0.7574	27.37	0.7703
Akiyo	CRNL	24.63	0.7013	26.56	0.7828	27.58	0.8208	28.27	0.8392	28.88	0.8530
Carphone	FCTN	28.17	0.7801	29.14	0.8118	29.55	0.8278	30.00	0.8394	30.51	0.8513
Coastguard	TNN	18.83	0.3412	21.31	0.4846	23.21	0.6025	24.83	0.6908	26.35	0.7630
Container	t-CTV	23.01	0.7172	25.63	0.8109	27.70	0.8648	29.41	0.9020	31.00	**0.9288**
Foreman	SCTR	**28.26**	**0.8186**	**30.81**	**0.8906**	**31.72**	**0.9066**	**32.14**	**0.9161**	**32.43**	0.9211
Color Images	LRTFR	13.72	0.1141	16.04	0.2182	14.99	0.3294	20.59	0.4400	22.53	0.5378
House	CRNL	19.73	0.4555	22.82	0.6450	24.66	0.7553	25.88	0.7898	26.96	0.8222
Peppers	FCTN	15.86	0.2374	17.40	0.3567	17.81	0.4052	18.25	0.4417	18.62	0.4667
Plane	TNN	14.52	0.2222	16.74	0.3350	18.45	0.4339	19.94	0.5209	21.26	0.5950
Sailboat	t-CTV	**20.95**	**0.6383**	22.93	**0.7249**	24.76	0.7906	25.89	0.8274	26.81	0.8506
Tree	SCTR	20.86	0.5434	**23.36**	0.6985	**25.25**	**0.8029**	**26.45**	**0.8532**	**27.78**	**0.8858**

Table 1: The average quantitative results by different methods for multi-dimensional data inpainting. Data dimensions: MSIs (256×256×31), Videos (144×176×900), Color Images (256×256×3). The **best** and second-best values are highlighted. (PSNR ↑, SSIM ↑)

maintaining computational efficiency through strategic parameter sharing, demonstrating consistent improvements across all tested scenarios.

Notations and Preliminaries

Throughout this paper, we use standard tensor notation where scalars, vectors, matrices, and tensors are denoted by lowercase letters (x), bold lowercase letters ($\mathbf{x}$), bold uppercase letters ($\mathbf{X}$), and calligraphic letters ($\mathcal{X}$), respectively. An N-th order tensor $\mathcal{X} \in \mathbb{R}^{I_1 \times I_2 \times \cdots \times I_N}$ has its $(i_1, i_2, \ldots, i_N)$-th element specified as $\mathcal{X}(i_1, i_2, \ldots, i_N)$.

The Frobenius norm of a tensor $\mathcal{X}$ is defined as $\|\mathcal{X}\|_F = \sqrt{\sum_{i_1,\ldots,i_N} |\mathcal{X}(i_1, \ldots, i_N)|^2}$. The mode-$n$ product of a tensor $\mathcal{X} \in \mathbb{R}^{I_1 \times \cdots \times I_N}$ with a matrix $\mathbf{A} \in \mathbb{R}^{J_n \times I_n}$, denoted by $\mathcal{Y} = \mathcal{X} \times_n \mathbf{A}$, yields a tensor of size $I_1 \times \cdots \times J_n \times \cdots \times I_N$.

The Proposed Method

Before illustrating our SCTR method, we first introduce related basic definitions and mechanisms.

Generalized Superpixel

Conventional Implicit Neural Representations (INRs) operate on individual pixels, struggling to capture higher-level semantic context. We introduce generalized superpixels as fundamental computational units—semantically coherent regions (Ren and Malik 2003; Kim, Park, and Shim 2023) that enable more effective integration of spatial and feature-level priors. This principle that semantically coherent regions possess stronger low-rank characteristics is central to our method. We formalize this concept through generalized superpixels—spatially connected regions with similar semantic content that serve as natural boundaries for local low-rank modeling.

Definition 1 (Generalized Superpixel)**.** *Motivation: We formalize superpixels as natural modeling units that respect semantic boundaries. Definition: Given a dataset $\mathcal{O} = \{\mathbf{o}_i \in \mathbb{R}^s\}_{i=1}^n$, a **generalized superpixel partition** $\{\mathcal{O}_k\}_{k=1}^K$ satisfies:*

1. ***Completeness**: $\bigcup_{k=1}^K \mathcal{O}_k = \mathcal{O}$ and $\mathcal{O}_k \cap \mathcal{O}_{k'} = \emptyset$ for $k \neq k'$*
2. ***Spatial Connectivity**: Each $\mathcal{O}_k$ forms a connected component in the spatial graph $G = (V, E)$ where vertices are data points and edges connect spatial neighbors*

Intuition: Unlike arbitrary partitions, superpixels respect natural image boundaries and exhibit stronger internal low-rank coherence, enabling more efficient tensor factorization.

Asymmetric Low-Rank Tensor Factorization (ALTF)

To effectively model continuous data while preserving the structural advantages of tensor decompositions, we first introduce the classical Tucker decomposition.

Definition 2 (Tucker Rank)**.** *The **Tucker rank** of a tensor $\mathcal{X} \in \mathbb{R}^{I_1 \times \cdots \times I_N}$ is the N-tuple of integers defined by the ranks of its mode-n matricizations:* $\text{rank}_T(\mathcal{X}) := (\text{rank}(\mathbf{X}^{(1)}), \text{rank}(\mathbf{X}^{(2)}), \ldots, \text{rank}(\mathbf{X}^{(N)}))$.

Theorem 1 (Tucker Decomposition)**.** *A tensor $\mathcal{X} \in \mathbb{R}^{I_1 \times \cdots \times I_N}$ can be factorized into a core tensor $\mathcal{C} \in \mathbb{R}^{R_1 \times \cdots \times R_N}$ and factor matrices $\{\mathbf{A}^{(n)} \in \mathbb{R}^{I_n \times R_n}\}_{n=1}^N$:* $\mathcal{X} \approx \mathcal{C} \times_1 \mathbf{A}^{(1)} \times_2 \mathbf{A}^{(2)} \cdots \times_N \mathbf{A}^{(N)}$.

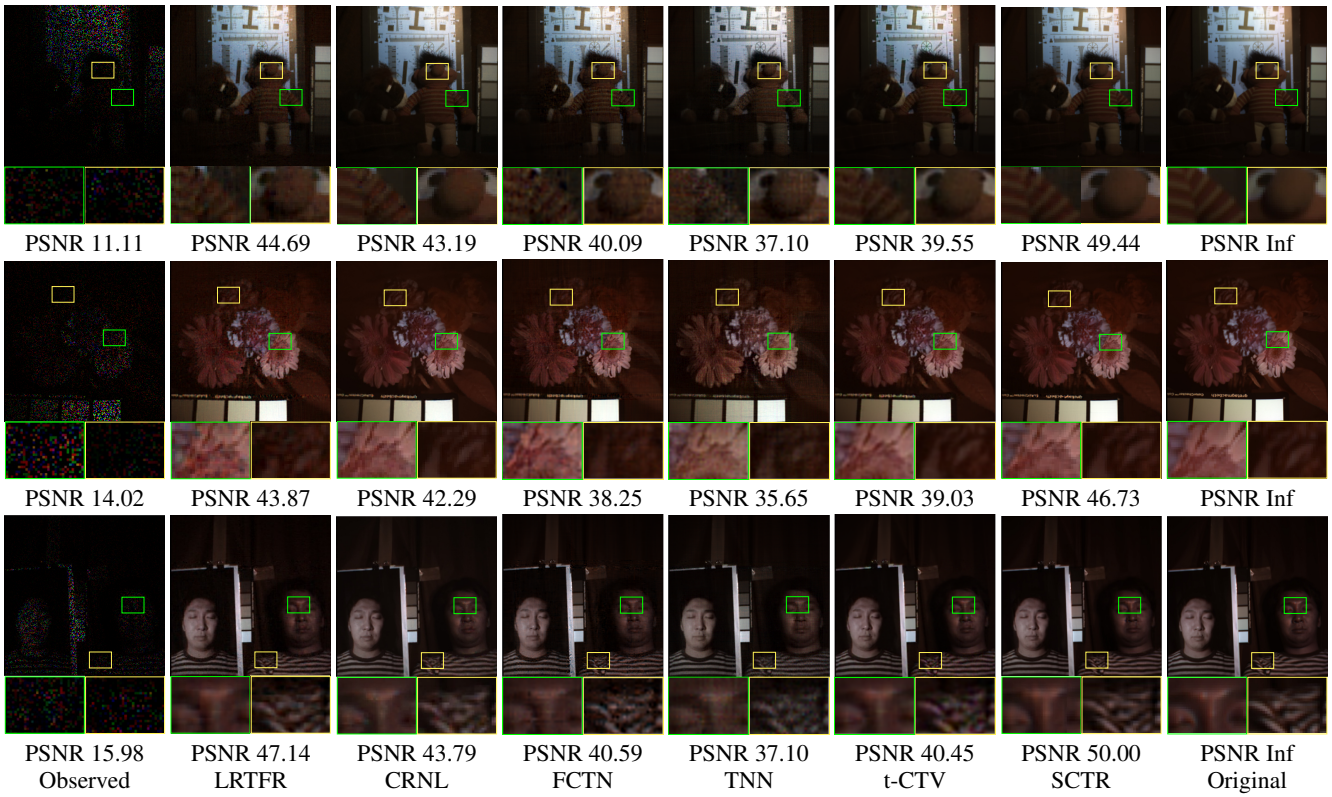


Figure 3: The results of multi-dimensional image inpainting by different methods on MSIs *Toy*, *Flowers*, and *Face* (SR = 0.15).

This classical formulation is designed for static, discrete data and relies on global low-rank assumptions. To address these challenges, we introduce Asymmetric Low-rank Tensor Factorization (ALTF). Traditional tensor decomposition treats all factor matrices equally. Our ALTF breaks this symmetry by generating factor matrices through a shared backbone with region-specific heads, achieving both parameter efficiency and representational flexibility.

Definition 3 (ALTF Parameterization)**.** *The ALTF mechanism models a continuous function $g_{\mathbf{\Theta}}$ which maps coordinates $\mathbf{c} = (c_u, c_v, c_w)$ to signal values. This function is parameterized by $\mathbf{\Theta} = \{\boldsymbol{\theta}_\Phi, \{\boldsymbol{\theta}_{\Psi k}\}_{k=1}^K, \{\mathcal{C}_k\}_{k=1}^K\}$, consisting of:*

1. *A deep, shared backbone network Φ with parameters $\boldsymbol{\theta}_\Phi$.*
2. *K patch-specific, lightweight head networks $\{\Psi_k\}_{k=1}^K$ with parameters $\boldsymbol{\theta}_{\Psi k}$.*
3. *K patch-specific core tensors $\{\mathcal{C}_k\}_{k=1}^K$.*

Factor matrices are generated from coordinate arrays via shared backbone and patch-specific heads: $\mathbf{U}_k = \Psi_k^U(\Phi(\mathbf{C}_u)) \in \mathbb{R}^{H_k \times R_1^k}$, where $\mathbf{C}_u = [c_1^u, ..., c_{H_k}^u]^T$ denotes the coordinate array.

where $\Phi(\cdot)$ denotes the shared backbone network and $\Psi_k^U(\cdot)$, $\Psi_k^V(\cdot)$, $\Psi_k^W(\cdot)$ represent the patch-specific head networks for generating factor matrices $\mathbf{U}_k$, $\mathbf{V}_k$, and $\mathbf{W}_k$, respectively.

The final reconstructed patch follows the Tucker decomposition:

$$\hat{\mathbf{X}}_k = \mathcal{C}_k \times_1 \mathbf{U}_k \times_2 \mathbf{V}_k \times_3 \mathbf{W}_k. \tag{1}$$

ALTF's key advantage stems from its architectural asymmetry. Compared to monolithic global INRs, ALTF captures fine-grained local details through patch-specific components. Compared to fully independent models, it is substantially more parameter-efficient by amortizing the backbone cost across patches, providing strong regularization for continuous data representation.

Superpixel-informed Continuous Low-Rank Tensor Representation

Building upon Generalized Superpixels (Definition 1) and Asymmetric Low-Rank Tensor Factorization (Definition 3), we propose the **Superpixel-informed Continuous Low-Rank Tensor Representation (SCTR)**. As shown in Figure2, SCTR operates in two stages: (1) superpixel segmentation using techniques like SLIC (Achanta et al. 2012) on a guide image generated by conventional methods (e.g., HaLRTC (Liu et al. 2013b)), and (2) patch-wise reconstruction via our Asymmetric Low-rank Tensor Factorization.

The model reconstructs each patch using an implicit neural network that maps 3D coordinates (x, y, z) to signal values through three key components: **(1) Global Shared SIREN Backbone**: A shared MLP with sinusoidal activations parameterizes factor matrices across all patches, re-



Figure 4: The results of video quantitative completion by different methods on videos *Akiyo*, *Coastguard*, and *Foreman* (SR = 0.1).

ducing parameters while learning global signal priors. **(2) Local Lightweight Heads**: Three separate linear heads (U, V, W) per patch predict factor matrices $\mathbf{U}_k$, $\mathbf{V}_k$, $\mathbf{W}_k$ from coordinate arrays for local adaptation. **(3) Learnable Core Tensor**: Each patch has a unique core tensor $\mathcal{C}_k \in \mathbb{R}^{r_1 \times r_2 \times r_3}$ capturing patch-specific low-rank structure.

The reconstructed patch k follows the Tucker decomposition:

$$\hat{\mathbf{X}}_k = \mathcal{C}_k \times_1 \mathbf{U}_k \times_2 \mathbf{V}_k \times_3 \mathbf{W}_k \tag{2}$$

where $\mathbf{U}_k$, $\mathbf{V}_k$, $\mathbf{W}_k$ are generated from coordinate arrays by the shared backbone and patch-specific heads.

The model is trained end-to-end using Adam optimizer to minimize MSE loss:

$$\min_{\Theta, \{\mathcal{C}_k\}} \sum_{k=1}^{K} \sum_{\mathbf{c} \in \Omega_k} \|\mathcal{F}_k(\mathbf{c}) - \mathcal{T}_k(\mathbf{c})\|_2^2, \tag{3}$$

where Θ represents shared backbone and head parameters, Ω_k contains observed coordinates in patch k, and $\mathcal{T}_k(\mathbf{c})$ is the ground-truth value. The complete training algorithm procedure is provided in the supplementary material.

Computational Complexity Analysis

For a 3D tensor $\mathcal{F} \in \mathbb{R}^{I_1 \times I_2 \times I_3}$ decomposed into K superpixels with dimensions (H_k, W_k, C_k) and Tucker ranks (R_1^k, R_2^k, R_3^k), SCTR's complexity per iteration is:

$$\mathcal{O}\Big(\sum_{k=1}^{K} \big[D^2(H_k + W_k + C_k) + D(H_k R_1^k + W_k R_2^k + C_k R_3^k) + H_k R_1^k R_2^k R_3^k + H_k W_k R_2^k R_3^k + H_k W_k C_k R_3^k \big] \Big) \tag{4}$$

where $D = 256$ is the backbone dimension. The terms represent: backbone forward pass, head projections, and Tucker reconstruction via sequential mode products.

With uniform ranks $R_i^k = R$ and average superpixel size $(\bar{H}, \bar{W}, \bar{C})$, this simplifies to $\mathcal{O}(K[D^2 n + DRn + \bar{H}\bar{W}\bar{C}R])$ where $n = \bar{H} + \bar{W} + \bar{C}$.

Compared to global Tucker with complexity $\mathcal{O}(I_1 I_2 I_3 R)$, SCTR's efficiency stems from: (i) local ranks $R^k \ll R_{\text{global}}$ due to superpixel homogeneity, (ii) amortized backbone cost across patches, and (iii) the condition $K\bar{H}\bar{W}\bar{C} \ll I_1 I_2 I_3$ ensuring computational advantage.

Experiments

We conduct comprehensive experiments across multiple data modalities including color images, multispectral images, and videos to evaluate SCTR's performance. Our method is compared against state-of-the-art approaches: LRTFR(Luo et al. 2024), t-CTV(Wang et al. 2023), TNN(Qin et al. 2022), FCTN(Zheng et al. 2021), and CRNL(Luo, Zhao, and Meng 2025).

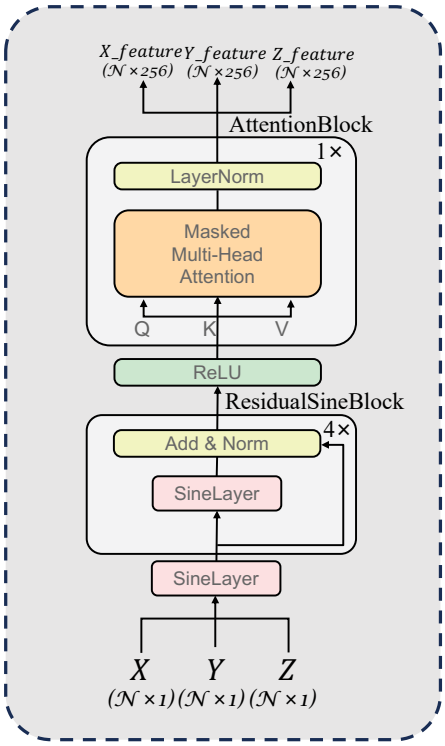


Figure 5: The architecture of our shared SIREN backbone. It processes 1D coordinates (X, Y, and Z, processed independently) through a SineLayer, four ResidualSineBlocks, a ReLU activation, and an AttentionBlock. This process maps each 1D coordinate vector of size $(N \times 1)$ to a feature vector of size $(N \times 256)$.

Experimental Setup. All experiments are conducted using PyTorch 2.5.1 and CUDA 11.8 on an RTX 3090 GPU. We employ Peak Signal-to-Noise Ratio (PSNR) and Structural Similarity Index Measure (SSIM) as evaluation metrics, where higher values indicate better reconstruction quality. Our model utilizes the Adam optimizer (Kingma and Ba 2015) with cosine annealing learning rate schedule(Loshchilov and Hutter 2017) and sinusoidal activation functions $\sigma(x) = \sin(\omega_0 x)$.

Hyperparameter Configuration. We train our model using the Adam optimizer with a cosine annealing learning rate schedule and a sinusoidal activation $\sigma(x) = \sin(\omega_0 x)$. For superpixel generation, we use 32 or 64 segments (compactness=10). Key hyperparameters are tuned via grid search, including: base learning rate ($[5 \times 10^{-5}, 5 \times 10^{-3}]$), weight decay ($[0.5, 3.0]$), SIREN frequency ω_0 ($[1, 5]$), and a coordinate downsampling factor $\mathbf{d}$ selected from $\{[1, 1, 1], [1, 2, 1], [2, 2, 1]\}$. The model is trained for 16k, 4k, and 3k iterations for MSIs, videos, and color images, respectively.

Multispectral Image Inpainting Results

We evaluate our SCTR method on multispectral image (MSI) inpainting using the CAVE dataset (Yasuma et al. 2010). As shown in Table 1 and Figure 3, our method demonstrates substantial improvements over existing approaches across all sampling rates. For MSI data at 15% sampling rate, SCTR achieves an average PSNR of 48.38 dB, outperforming the second-best method (LRTFR) by 3.73 dB. This significant improvement can be attributed to our superpixel-based approach, which effectively captures the inherent low-rank structure within semantically coherent regions.

The visual results in Figure 3 further validate our approach. While baseline methods such as TNN and FCTN struggle with preserving fine details, our method maintains sharp edges and accurate color reproduction across diverse MSI content.

Video Inpainting Results

For video inpainting evaluation, we utilize five standard sequences from the Arizona State University (ASU) video trace library. As presented in Table 1 and Figure 4, SCTR consistently outperforms competing methods across different video types and sampling rates. At 10% sampling rate, our method achieves an average PSNR of 30.81 dB with SSIM of 0.8906, representing gains of 1.67 dB and 0.0788 SSIM over the second-best performing FCTN method.

The superiority of SCTR is particularly pronounced in videos with complex motion patterns. Our method effectively maintains temporal coherence while preserving spatial details, as demonstrated by the comparisons in Figure 4.

Color Image Inpainting Results

We further validate SCTR on the USC-SIPI Image Database . As shown in Table 1 and Figure 6, our method achieves competitive performance even on traditional RGB data. At 15% sampling rate, SCTR attains an average PSNR of 25.25 dB with SSIM of 0.8029, exceeding the performance of t-CTV while significantly outperforming other tensor-based methods.

While the performance gap is smaller compared to MSI and video data—likely due to reduced spectral redundancy in RGB images—our unified framework still provides consistent improvements, demonstrating the versatility of combining superpixel segmentation with ALTF across different data modalities.

Ablation Study

Component Analysis

To validate the contributions of SCTR's key components, we conducted an ablation study on the CAVE dataset, including *toy*, *beers*, with 10% sampling rate. As shown in Table 2, the full SCTR model achieves a PSNR of 46.66 dB. Removing either the superpixel-based modeling or the ALTF mechanism leads to a significant performance drop of 4.54 dB and 3.17 dB, respectively. This confirms both components are essential for the model's state-of-the-art performance.

Semantic Granularity Analysis

We investigate optimal superpixel density for SCTR by validating that reconstruction quality follows information-theoretic principles.

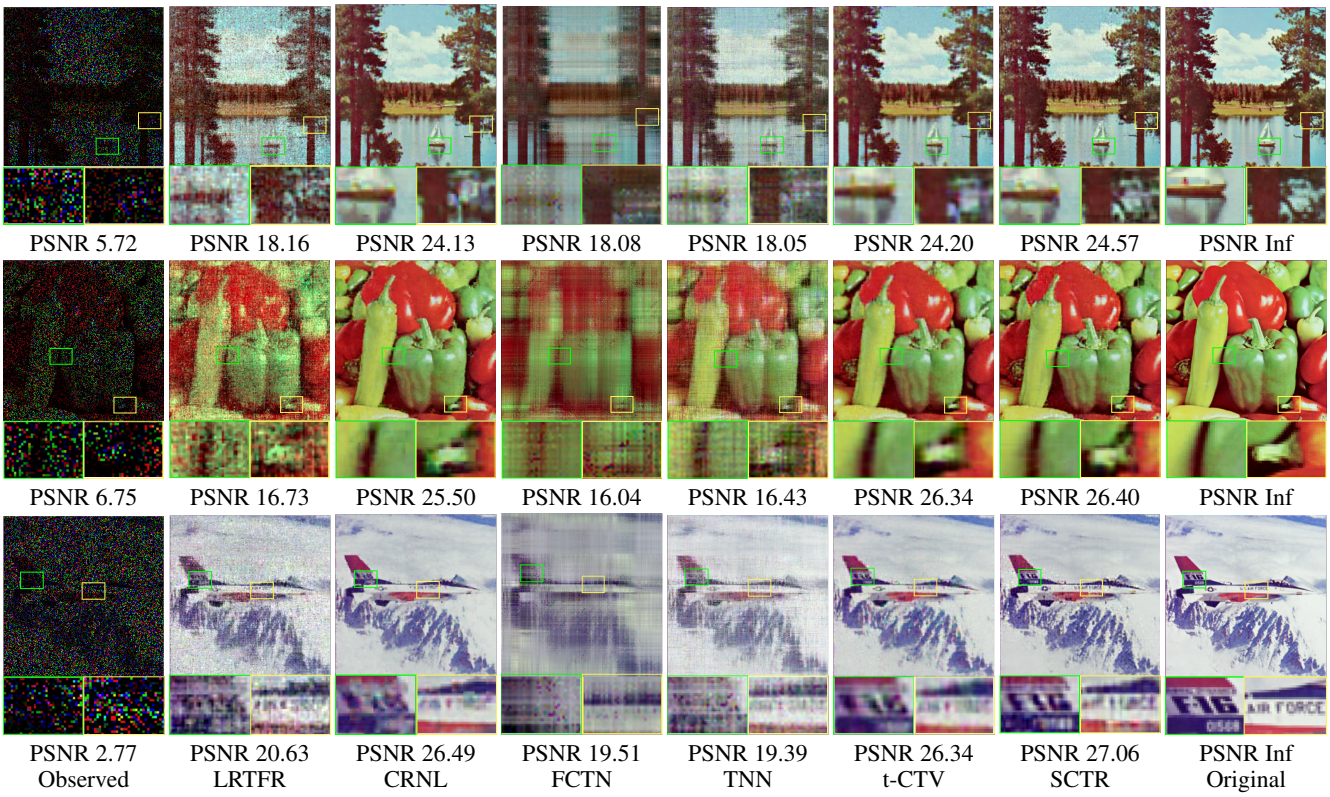


Figure 6: The results of multi-dimensional image inpainting by different methods on color images *Sailboat*, *Peppers*, and *Plane* (SR = 0.15).

Components		MSIs (SR=10%)	
Superpixel	ALTF	PSNR	SSIM
×	×	39.11	0.9367
×	✓	42.12	0.9703
✓	×	43.49	0.9685
✓	✓	**46.66**	**0.9956**

Table 2: Ablation study of our two main components on the MSI dataset (10% sampling rate). The best results are highlighted in **bold**.

Theoretical Framework. Optimal reconstruction occurs when superpixel granularity $\mathcal{G}$ balances semantic coherence with computational efficiency:

$$\mathcal{G}^* = \arg\min_{\mathcal{G}} \underbrace{\mathbb{E}[\mathcal{H}(\text{intra-patch})]}_{\text{semantic entropy}} + \underbrace{\lambda \cdot \mathcal{C}(\mathcal{G})}_{\text{computational cost}} \tag{5}$$

Experimental Validation. Using granularity coefficient α where $N = 8 \times 2^{\alpha}$ superpixels, we tested on the *Akiyo* sequence:

Key Findings. The results in Table 3 show that performance improves significantly as superpixel count increases from 8 to 32, but the gains diminish thereafter. This suggests that using 32 or 64 segments offers the best trade-off between reconstruction quality and computational cost, validating our local modeling approach.

α	Superpixels N	PSNR (dB)	SSIM
0.0	8	27.93	0.8247
1.0	16	29.46	0.8793
2.0	32	30.25	0.8997
2.5	48	31.34	0.9219
3.0	64	32.09	0.9407
3.3	80	32.23	0.9402

Table 3: Impact of semantic granularity on reconstruction quality.

The logarithmic relationship confirms SCTR effectiveness depends on semantic homogeneity within superpixels, with each granularity doubling providing fixed information gain consistent with hierarchical semantic processing.

Conclusion

We introduced SCTR, a framework that overcomes the limitations of classical tensor methods by modeling semantically coherent superpixels with a continuous, Asymmetric Low-rank Tensor Factorization (ALTF). Extensive experiments show SCTR consistently outperforms state-of-the-art methods, yielding significant PSNR gains of up to 5 dB on multispectral image recovery. Ablation studies confirm that

both the superpixel-based local modeling and the ALTF architecture are essential for this performance. By effectively bridging the discrete-continuous divide in tensor modeling, SCTR opens new avenues for high-fidelity representation of complex signals, with strong implications for tasks like neural radiance field analysis and point cloud processing.

References

Achanta, R.; Shaji, A.; Smith, K.; Lucchi, A.; Fua, P.; and Süsstrunk, S. 2012. SLIC Superpixels Compared to State-of-the-Art Superpixel Methods. *IEEE Transactions on Pattern Analysis and Machine Intelligence*, 34(11): 2274–2282.

Bengua, J. A.; Phien, H. N.; Tuan, H. D.; and Do, M. N. 2017. Efficient Tensor Completion for Color Image and Video Recovery: Low-Rank Tensor Train. *IEEE Transactions on Image Processing*, 26(5): 2466–2479.

Chen, A.; Xu, Z.; Geiger, A.; Yu, J.; and Su, H. 2022. TensoRF: Tensorial Radiance Fields. In *European Conference on Computer Vision (ECCV)*.

Chen, H.; He, B.; Wang, H.; Ren, Y.; Lim, S.; and Shrivastava, A. 2021. NeRV: Neural Representations for Videos. In Ranzato, M.; Beygelzimer, A.; Dauphin, Y. N.; Liang, P.; and Vaughan, J. W., eds., *Advances in Neural Information Processing Systems 34: Annual Conference on Neural Information Processing Systems 2021, NeurIPS 2021, December 6-14, 2021, virtual*, 21557–21568.

Chen, Y.; Liu, S.; and Wang, X. 2021. Learning continuous image representation with local implicit image function. In *Proceedings of the IEEE/CVF Conference on Computer Vision and Pattern Recognition*, 8628–8638.

Essakine, A.; Cheng, Y.; Cheng, C.; Zhang, L.; Deng, Z.; Zhu, L.; Schönlieb, C.; and Avilés-Rivero, A. I. 2025. Where Do We Stand with Implicit Neural Representations? A Technical and Performance Survey. *Trans. Mach. Learn. Res.*, 2025.

Gong, X.; Chen, W.; and Chen, J. 2020. A Low-Rank Tensor Dictionary Learning Method for Hyperspectral Image Denoising. *IEEE Transactions on Signal Processing*, 68: 1168–1180.

Jiang, J.; Xu, Y.; Xu, H.; Shen, G.; and Zheng, J. 2024. Multi-dimensional visual data completion via weighted hybrid graph-Laplacian. *Signal Processing*, 216: 109305.

Jiang, T.-X.; Ng, M. K.; Zhao, X.-L.; and Huang, T.-Z. 2020. Framelet Representation of Tensor Nuclear Norm for Third-Order Tensor Completion. *IEEE Transactions on Image Processing*, 29: 7233–7244.

Kilmer, M. E.; and Martin, C. D. 2011. Factorization strategies for third-order tensors. *Linear Algebra and its Applications*, 435(3): 641–658.

Kim, S.; Park, D.; and Shim, B. 2023. Semantic-Aware Superpixel for Weakly Supervised Semantic Segmentation. *Proceedings of the AAAI Conference on Artificial Intelligence*, 37(1): 1142–1150.

Kingma, D. P.; and Ba, J. 2015. Adam: A Method for Stochastic Optimization. In Bengio, Y.; and LeCun, Y., eds., *3rd International Conference on Learning Representations, ICLR 2015, San Diego, CA, USA, May 7-9, 2015, Conference Track Proceedings*.

Kolda, T. G.; and Bader, B. W. 2009. Tensor Decompositions and Applications. *SIAM Review*, 51(3): 455–500.

Li, J.; Zhao, X.; Wang, J.; Wang, C.; and Wang, M. 2024. *Superpixel-Informed Implicit Neural Representation for Multi-dimensional Data*, 258–276. Springer Nature Switzerland.

Li, X. P.; and So, H. C. 2021. Robust Low-Rank Tensor Completion Based on Tensor Ring Rank via $\ell_{p,\epsilon}$-Norm. *IEEE Transactions on Signal Processing*, 69: 3685–3698.

Liu, J.; Musialski, P.; Wonka, P.; and Ye, J. 2013a. Low-rank matrix recovery via convex optimization. *ACM Transactions on Graphics*, 32(4): 1–13.

Liu, J.; Musialski, P.; Wonka, P.; and Ye, J. 2013b. Tensor Completion for Estimating Missing Values in Visual Data. *IEEE Transactions on Pattern Analysis and Machine Intelligence*, 35(1): 208–220.

Liu, S.; Zhao, X.-L.; Leng, J.; Li, B.-Z.; Yang, J.-H.; and Chen, X. 2024. Revisiting High-Order Tensor Singular Value Decomposition From Basic Element Perspective. *IEEE Transactions on Signal Processing*, 72: 4589–4603.

Liu, Y.; Yuan, X.; Suo, J.; Brady, D. J.; and Dai, Q. 2019. Rank Minimization for Snapshot Compressive Imaging. *IEEE Transactions on Pattern Analysis and Machine Intelligence*, 41(12): 2990–3006.

Loshchilov, I.; and Hutter, F. 2017. SGDR: Stochastic Gradient Descent with Warm Restarts. In *5th International Conference on Learning Representations, ICLR 2017, Toulon, France, April 24-26, 2017, Conference Track Proceedings*. OpenReview.net.

Luo, Y.; Zhao, X.; Li, Z.; Ng, M. K.; and Meng, D. 2024. Low-Rank Tensor Function Representation for Multi-Dimensional Data Recovery. *IEEE Transactions on Pattern Analysis and Machine Intelligence*, 46(5): 3351–3369.

Luo, Y.; Zhao, X.; and Meng, D. 2025. Revisiting Nonlocal Self-Similarity from Continuous Representation. *IEEE Transactions on Pattern Analysis and Machine Intelligence*, 47(1): 450–468.

Newman, E.; Horesh, L.; Avron, H.; and Kilmer, M. E. 2024. Stable tensor neural networks for efficient deep learning. *Frontiers in Big Data*, 7.

Oseledets, I. V. 2011. Tensor-Train Decomposition. *SIAM Journal on Scientific Computing*, 33(5): 2295–2317.

Park, K.; Sinha, U.; Barron, J. T.; Bouaziz, S.; Goldman, D. B.; Seitz, S. M.; and Martin-Brualla, R. 2021. Nerfies: Deformable neural radiance fields. In *Proceedings of the IEEE/CVF International Conference on Computer Vision*, 5865–5874.

Qin, W.; Wang, H.; Zhang, F.; Wang, J.; Luo, X.; and Huang, T. 2022. Low-Rank High-Order Tensor Completion With Applications in Visual Data. *IEEE Transactions on Image Processing*, 31: 2433–2448.

Ren, X.; and Malik, J. 2003. Learning a classification model for segmentation. In *Proceedings Ninth IEEE International Conference on Computer Vision*, 10–17 vol.1.

Sitzmann, V.; Martel, J. N. P.; Bergman, A. W.; Lindell, D. B.; and Wetzstein, G. 2020. Implicit Neural Representations

with Periodic Activation Functions. In Larochelle, H.; Ranzato, M.; Hadsell, R.; Balcan, M.; and Lin, H., eds., *Advances in Neural Information Processing Systems 33: Annual Conference on Neural Information Processing Systems 2020, NeurIPS 2020, December 6-12, 2020, virtual*.

Sitzmann, V.; Zollhöfer, M.; and Wetzstein, G. 2019. Scene Representation Networks: Continuous 3D-Structure-Aware Neural Scene Representations. In Wallach, H. M.; Larochelle, H.; Beygelzimer, A.; d'Alché-Buc, F.; Fox, E. B.; and Garnett, R., eds., *Advances in Neural Information Processing Systems 32: Annual Conference on Neural Information Processing Systems 2019, NeurIPS 2019, December 8-14, 2019, Vancouver, BC, Canada*, 1119–1130.

Vemuri, S. K.; Büchner, T.; and Denzler, J. 2025. F-INR: Functional Tensor Decomposition for Implicit Neural Representations. *CoRR*, abs/2503.21507.

Wang, H.; Peng, J.; Qin, W.; Wang, J.; and Meng, D. 2023. Guaranteed Tensor Recovery Fused Low-rankness and Smoothness. *IEEE Transactions on Pattern Analysis and Machine Intelligence*, 45(9): 10990–11007.

Wang, M.; Pan, Y.; Xu, Z.; Li, G.; Yang, X.; Mandic, D.; and Cichocki, A. 2025. Tensor Networks Meet Neural Networks: A Survey and Future Perspectives. arXiv:2302.09019.

Wang, W.; Aggarwal, V.; and Aeron, S. 2017. Efficient Low Rank Tensor Ring Completion. In *2017 IEEE International Conference on Computer Vision (ICCV)*, 5698–5706.

Yasuma, F.; Mitsunaga, T.; Iso, D.; and Nayar, S. K. 2010. Generalized Assorted Pixel Camera: Postcapture Control of Resolution, Dynamic Range, and Spectrum. *IEEE Transactions on Image Processing*, 19(9): 2241–2253.

Zhang, H.; and Zheng, B. 2025. Low-Rank Tensor Completion via Tensor Joint Rank With Logarithmic Composite Norm. *Numer. Linear Algebra Appl.*, 32(2).

Zhang, Z.; Ely, G.; Aeron, S.; Hao, N.; and Kilmer, M. 2014. Novel methods for multilinear data completion and de-noising based on tensor-SVD. In *Proceedings of the IEEE Conference on Computer Vision and Pattern Recognition*, 3842–3849.

Zhao, L.; Xu, X.; Wang, Z.; Zhang, Y.; Zhang, B.; Zheng, W.; Du, D.; Zhou, J.; and Lu, J. 2024. LowRankOcc: Tensor Decomposition and Low-Rank Recovery for Vision-Based 3D Semantic Occupancy Prediction. In *2024 IEEE/CVF Conference on Computer Vision and Pattern Recognition (CVPR)*, 9806–9815.

Zheng, Y.-B.; Huang, T.-Z.; Zhao, X.-L.; Zhao, Q.; and Jiang, T.-X. 2021. Fully-Connected Tensor Network Decomposition and Its Application to Higher-Order Tensor Completion. *Proceedings of the AAAI Conference on Artificial Intelligence*, 35(12): 11071–11078.